Sensors & Transducers, Vol. 162 , Issue 1, January 2014, pp. 273-279

www.sensorsportal.com

Sensors & Transducers

© 2014 by IFSA Publishing, S. L.
http://www.sensorsportal.com

Structure Optimization and Performance Analysis of SRM with Amorphous Alloys Core using FEM

Yiduan CHEN, Huijuan LIU, Jingxiong ZHANG
School of Electrical Engineering, Beijing Jiaotong University, Beijing, 100044, China
Tel.: 010-51684831, fax: 010-51687101
E-mail: duanduan_happy90@163.com

Received: 16 October 2013 /Accepted: 9 January 2014 /Published: 31 January 2014

Abstract: This paper presents the performance computation of three-phase 6/4 poles Switched Reluctance Motor (SRM) with amorphous alloy core using transient Finite Element Analysis (FEA) in which the magnetic field is combined with a driving circuit. In order to minimize torque ripple in SRM, this paper proposes not only optimal combination of stator pole arc and rotor pole arc but also the turn-on and turn-off angles using parameterized transient FEA and response surface methodology (RSM). The magnetic fields distribution, the winding flux linkage, the phase inductance curve, the iron losses and the torque characteristics of the prototype SRM at low-speed are investigated. All studies show that the prototype SRM is potential to apply in home appliance applications. *Copyright © 2014 IFSA Publishing, S. L.*

Keywords: Switched reluctance motor (SRM), Amorphous alloys core, Finite element analysis (FEA), Response surface methodology (RSM), Parameterized transient FEA.

1. Introduction

The switched reluctance machines (SRM) have been extensively investigated and developed in the past decades by several research organizations [1-3]. There are several advantages in SRMs such as rotor robustness, low cost and possible operation in high temperatures or high rotational speeds. Cooling is easy because most of the heat generation occurs in the stator. Thanks to the salient rotor structure, a torque/inertia ratio is high. Thus, fast acceleration and deceleration can be realized with low load inertia. SRMs have been used extensively in home appliances and employed in many different industrial applications [4-5]. It is recognized that efficiency of SRM is rather low, in general, compared with the permanent magnet machines. Improving the motor efficiency is an important project for promoting applications of SRM.

Fig. 1 shows a general efficiency of various motors with respect to power ratings. The curves IM and SRM indicate relationships of efficiency and rated powers of Y2 series high efficiency 4-pole induction motors [6] and SRM respectively. Note that efficiency is high in high power motors. In a few kW motors efficiency is generally less than 80 %.

There are two basic methods to increase a motor's efficiency, the one is to decrease the losses in the motor; the other is to increase the output of the motor.

The first efficiency improvement method is achieved by some techniques such as to improve the manufacturing process and use new materials (Fe-based amorphous alloys), to develop the optimal control strategy and optimal voltage waveforms, etc.

On the other hand, more and more functions were added to products for home appliances, industrial machines and automotives to meet customer needs,

which left less space for motors. Therefore, smaller size is also required for many motor applications. A motor's output can be defined as the product of torque and the rotating speed. One typical way to construct a larger output motor without increasing a motor's size is to increase a motor's rotational speed. Recently, home appliances, industrial machines and automobiles began being developed using motors that operate at speeds of 5000 r/min or greater in the actuators [7]. However, high rotational speed means high frequency electromagnetic fields in the rotor or stator, which cause larger core losses produced by magnetic materials. Therefore, the performances of soft magnetic materials at high frequencies are expected to improve. The low core loss magnetic materials, Fe-based amorphous alloys have drawn attention due to their excellent magnetic properties. Table 1 provides the characteristics of 0.5 mm Si-Fe sheet and Fe-based amorphous alloys [8-10].

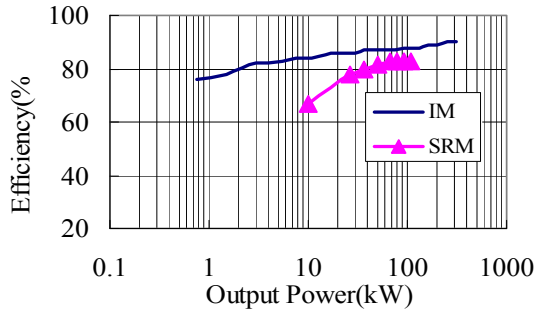

Fig. 1. Efficiency versus output of various motors.

Table 1. Characteristics of Si-Fe Sheet and Fe-based amorphous alloy.

Item	Si-Fe sheet (DW360)	Fe-based amorphous alloy
Density	7.65 g/cm3	7.18 g/cm3
Thickness	0.5 mm	0.025 mm
B(9000A/m)	1.72 T	1.56 T
Specific Resistance	0.82 μΩ.m	1.37 μΩ.m
Loss (1.45T,50Hz)	2.8 W/kg	0.22 W/kg
Vickers hardness	200~300	900
Permeability μmax	4×104 H/m	25×104 H/m
Coercivity Hc	4 A/m	30 A/m

Amorphous alloys, also known as metallic glass, which has features of extremely low iron losses, high magnetic permeability, and high fracture toughness. Compared to silicon steel sheet, they produce less eddy-current loss when the metal is subjected to an alternating magnetic field because of their high resistance. Amorphous alloys also produce low hysteresis loss due to their disordered atomic structure. These excellent properties offer great possibilities to increase motor efficiency using amorphous alloys [11, 12].

In this paper a comparison is presented for constructed sample SRMs with Fe-based amorphous alloys materials for home appliance applications at low-speed operation.

With the help of response surface methodology (RSM) and the parameterized transient finite element analysis model of the sample SRM, the stator pole arc β_s, rotor pole arc β_r, the turn-on angle θ_{on} and turn-off angle θ_{off} of the sample SRM are optimized for reducing torque ripple.

The performance is presented for the sample SRM by using finite element analysis. The magnetic fields distribution, the torque and the terminal characteristics of the prototype SRM with same size at low-speed are presented. The iron losses, the copper losses and efficiency of amorphous iron SRM are compared with traditional silicon steel SRM.

2. Iron Material and Motor Targets

Magnetic characteristic of iron cores are particularly important because SRMs do not have a permanent magnet. Fig. 2 shows a comparison of B-H curves. The saturated flux density of conventional silicon steel DW360 is better than that of Fe-based amorphous alloy. The permeability at unsaturated region is better in Fe-based amorphous alloy.

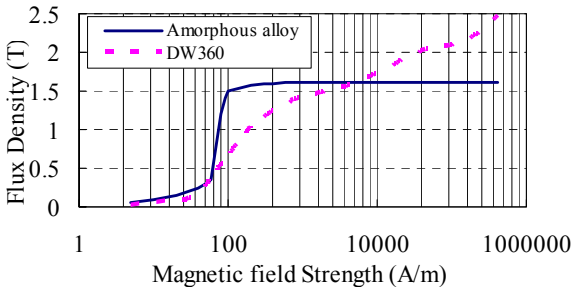

Fig. 2. B-H curves of silicon steel (DW360) and Fe-based amorphous alloy.

Fig. 3 shows a comparison of iron loss curves provided by steel manufactures. Iron loss characteristic of the Fe-based amorphous alloy is excellent. When iron loss of DW360 at 1.0T (50 Hz) is assumed to be 100 % (2.1 W/kg), iron loss of Fe-based amorphous alloy is about 5 % (0.1 W/kg).

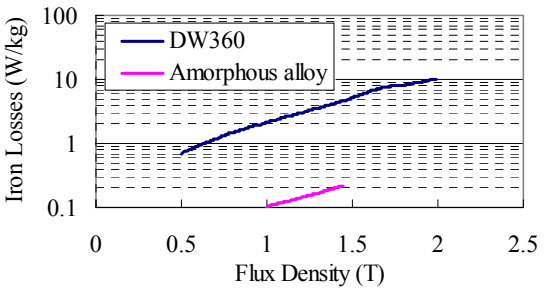

Fig. 3. Iron losses versus flux density for silicon steel (DW360) and Fe-based amorphous alloy at 50 Hz.

We will develop sample SRM (three-phase 6/4 poles) with amorphous alloy core and silicon steel core at speed 100 r/min respectively. The motors obtained 100 W output at 100 r/min with a size of Φ160×L70, and the rated torque is 10 Nm.

3. Optimal Design of Pole Arcs and Switching Angles

Designing SRM especially for high performance motion control systems requires accurate knowledge of the magnetic fields that relate motor geometry and motor performance. These relationships can be investigated through extensive prototyping, which is impractical and very costly, or by accurate magnetic field simulations. Magnetic field simulation directly yields predictions of flux linkages, field energy, and torque [13, 14].

In order to design the target SRM (three-phase 6/4 SRM) to meet the low torque ripple and large torque density in home appliance, two design parameters should be considered, one is geometrically parameter such as pole arcs (stator pole arc β_s and rotor pole arc β_r), and another is significant electric parameter such as switching angles (turn-on angle θ_{on} and turn-off angle θ_{off}). If the sample SRM is analyzed with the variation of pole arcs (β_s and β_r) in the fixed switching angle, it is hard to obtain good performance. Therefore, the drive condition, especially the turn-on angle θ_{on} and turn-off angle θ_{off} also should be considered when designing SRM.

Fig. 4 shows excitation scheme considered in this paper. Inductance profile varies with the combination of stator and rotor pole arcs, and the torque performances are influenced by the combination of inductance characteristic and switching angle.

The condition of θ_{on} is that the flat-topped current has to flow at the starting point of rising-inductance. The condition of θ_{off} is that the current should be zero at the starting point of falling-inductance, and the conduction angle $p_w=\theta_{off}-\theta_{on}$.

If the pole arcs of stator and rotor are smaller and switching angle θ_{off} coincides with the starting point of rising-inductance, a large torque ripple will be periodically generated as shown in Fig. 4(a). It is also impossible to reduce torque ripple although the phase current flows ideally. So the case of Fig. 4(a) is not considered in this paper. The design and switching schemes in Fig. 4(b) demonstrate that if the conduction angle p_w is increased, i.e., the switching angle θ_{on} is decreased, and the pole arcs are widened, the torque ripple can be minimized. From Fig. 4(b), we can find that to widen the rotor pole arc β_r is better than to widen the stator pole arc β_s with respect of space factor, magneto motive force and average torque.

In this paper, the parameterized transient finite element analysis model of the sample SRM is developed to sweep the pole arcs and switching angles, aiming to minimize the torque ripple. There are totally three design parameters $\{p\}=\{\beta_s, \beta_r, p_w\}$ to sweep for the design analysis, the mentioned pole arcs β_s and β_r and the conduction angles p_w in SRM are optimized efficiently with the help of response surface methodology (RSM). As an accepted effective approach, RSM is usually applied for searching the optimal design of electrical devices in order to improve machine performances. It is a set of statistical and mathematical techniques to find the "best fitted" response of the physical system through simulation [8].

According to [15], the relationship between β_s and β_r can be expressed as:

$$\begin{cases} \beta_s = (0.3 \sim 0.42) \times 90 \,\text{deg ree} \\ \beta_r = (0.9 \sim 1.4) \times \beta_s \,\text{deg ree} \end{cases}, \tag{1}$$

The relationship between stator pole width b_s and rotor pole width b_r can be written as:

$$\begin{cases} b_s = 2 \times (D_{si}/2) \times \sin(\beta_s/2) \ \text{mm} \\ b_r = 2 \times (D_r/2) \times \sin(\beta_r/2) \ \text{mm} \end{cases}, \tag{2}$$

where D_{si} is the inner diameter of the stator, D_r is the outer diameter of the rotor, and in the sample SRM, D_{si} =83 mm, D_r =82 mm.

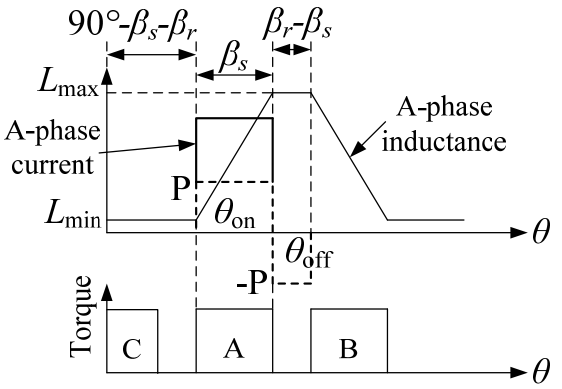

(a) θ_{on} coincides with the starting point of rising-inductance

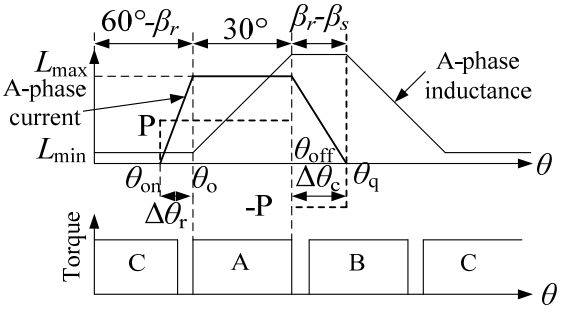

(b) θ_{on} is smaller than the starting point of rising-inductance

Fig. 4. Torque generation with pole arcs and switching angle combinations.

Therefore, in the sample motor, the range of β_s and b_s are 27 degree ≤ β_s ≤ 37.8 degree and 19.38 mm ≤ b_s ≤ 26.38 mm respectively. And accordingly, the range of β_r and b_r can be obtained according to Eq. 1 and Eq. 2. The range of p_w is 30 degree ≤ p_w ≤ 39 degree.

The torque performance of SRM is also influenced by the inductance profile, i.e. the rotor position θ_r (Fig. 4). A parameterized transient finite element analysis model of the sample SRM is built to compute the torque curves when b_s, b_r, p_w and θ_r are changing. For all the parameters in the sweeping analysis, uniform steps are used to solve for the optimal design such that 1mm for parameters b_s and b_r, 1 degree for p_w and 1.2 degree for θ_r as shown in Table 2, so there are totally 8×7×10×28=15680 times FEM computations. In our FEA parameter sweeping computation, it takes around 15 hours to obtain all the solutions.

15680 sample points are computed using FEM, and the torque as a function of the parameters {b_s, b_r, p_w, θ_r} is reconstructed by the response surface method with multi-quadratics basis function.

Table 2. Variable Range.

Parameters	Range	Step
β_s (degree)	27.01~37.06	1
b_s(mm)	19.38~26.38	1
p_w (degree)	30~39	1
θ_r(degree)	0~33.6	1.2

Torque versus the parameters {b_r, p_w, θ_r} is shown in Fig. 5; and torque versus the parameters {b_s, b_r, θ_r} is shown in Fig. 6.

Then, by using response surface methodology (RSM), the optimal b_s, b_r and p_w of the sample SRM is determined: stator pole width b_s =20.38 mm, rotor pole width b_r =22.10 mm, conduction angle p_w =31 degree, accordingly, the optimal β_s and β_r of the sample SRM are 28.43 degree and 31.27 degree respectively.

Fig. 7 shows the cross section of sample SRM.

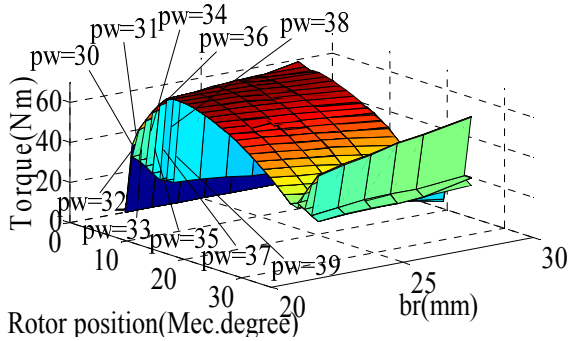

Fig. 5. Torque versus b_r, p_w and θ_r.

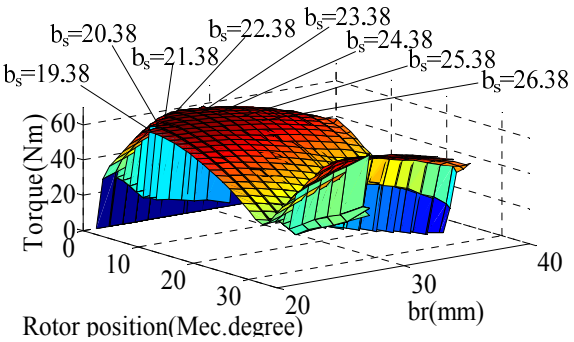

Fig. 6. Torque versus b_s, b_r and θ_r.

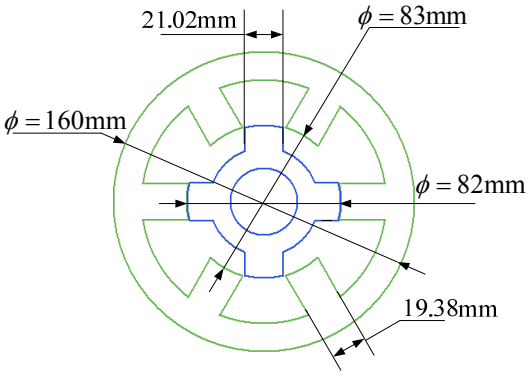

Fig. 7. The shape of iron cores.

4. Finite Element Analysis of Sample SRM

In order to obtain an accurate motor design, the 2D finite element analysis (FEA) was used to compute the performances of sample SRM with Fe-based amorphous alloy material.

4.1. Winding Flux Linkages

In SRM, when a stator pole is opposite a rotor pole is defined as the aligned position such that the reluctance of the motor magnetic structure is minimum. This location is assumed to be as 90 electrical degrees for the rotor position in the motors performance plots. The unaligned position (zero electrical degree) is defined as that when the rotor pole is in opposite the stator slot such that the reluctance of the motor magnetic structure is at its maximum. In the analysis the rotor moves from unaligned to aligned positions.

The reluctance variation of SRM has an important role on its performance; hence an accurate knowledge of the flux linkage of the motor for different excitation currents and rotor positions is essential for the prediction of motor performance.

In Fig. 8, the flux linkage of one phase is represented as a function of excitation current for the extreme position, unaligned and aligned position.

In silicon steel motor, the amount of flux linkage of one phase is increased compared with the amorphous alloy motor at high current in aligned position, but in unaligned position, owing to the magnetic circuit is linear; the flux linkage of silicon steel SRM is same as that of Fe-based amorphous alloy SRM.

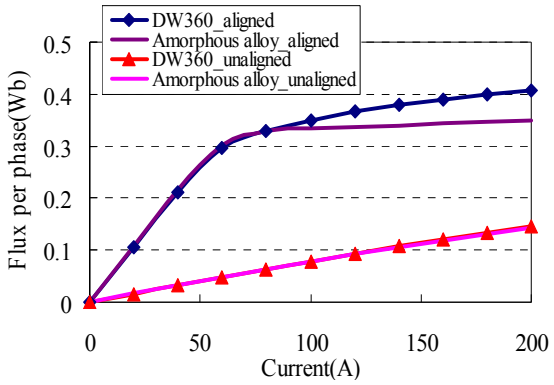

Fig. 8. The phase flux as a function of current (DW360, Fe-based amorphous alloy).

4.2. Phase Inductance Curves

The inductance (L) has been defined as the ratio of each phase flux linkages to the exciting current. Values based on this definition for sample SRM with Fe-based amorphous alloy material are presented in Fig. 9.

In Fig. 9, zero degree is considered to be as the unaligned case. In the aligned position the inductance is greatest at low values of excitation current and decreases as the motor goes into unaligned position. This inductance reduction is due to the fact that the reluctance of the motor magnetic circuit increases as the rotor moves into the unaligned position. At higher current levels the inductance variation is less sensitive to the rotor position.

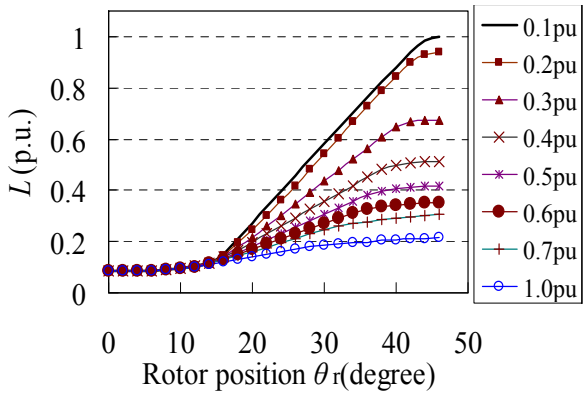

Fig. 9. The phase inductances as a function of rotor position.

4.3. Magnetic Field Distribution

For all motors the field solutions are obtained at the aligned and unaligned positions. The motor is highly saturated under normal operating conditions. The plots of magnetic flux density throughout the motors have been obtained and are shown in Fig. 10.

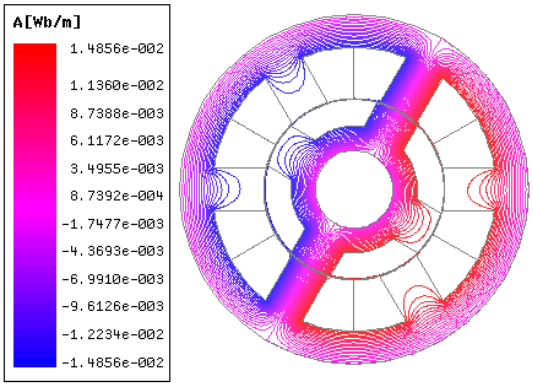

(a) Aligned position

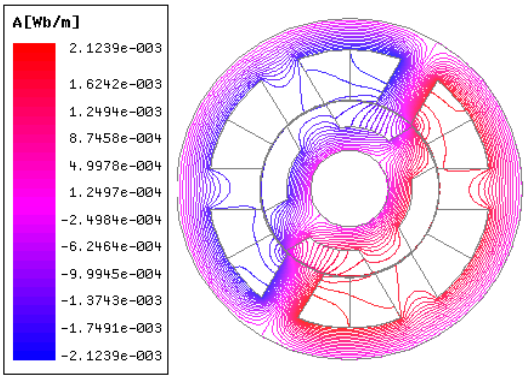

(b) Unaligned position

Fig. 10. Flux distribution when one phase is excited for Fe-based amorphous alloy.

4.4. Torque Capability

As the magnetic coupling between phases is negligible, one considers that the self-inductance variation is the only origin of torques. Indeed, in switched reluctance motor, the electromagnetic torque is obtained by deriving self-inductance and multiplying by square of current.

$$T = i^2 \frac{\partial L(\theta_r, i)}{\partial \theta_r}, \tag{3}$$

where T is the electromagnetic torque, L is the phase self-inductance, θ_r is the rotor position and i is the phase current.

So, comparing the self-inductances variations versus rotor position is indispensable.

The figure shows the variations of these inductances as a function of the position (in electrical degrees) for both motors. To see the influence of saturation, several current values are considered.

At low current, in absence of magnetic saturation the inductance variation is conditioned mainly by the magnetic geometry of the structure.

The nonlinear variation of inductance in the SRMs induces probably some additional torque ripples. This nonlinearity (due to the geometry and saturation) makes also its analytical modeling more difficult.

To compare the electromechanical conversion, one considers electromagnetic torques developed when the given supply voltage is 190 V. The shapes of transient torques are shown in the Fig. 11.

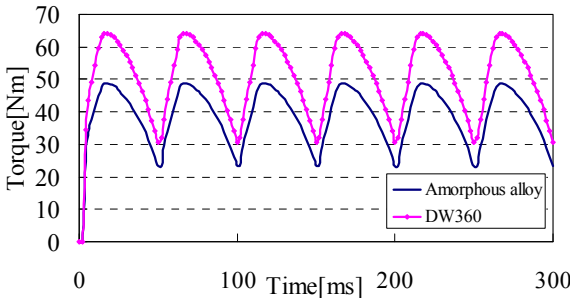

Fig. 11. Torque versus time.

The SRMs torque is directly linked to the derivatives of inductances, not directly to the inductance shape. So, any dissimilitude in this derivative shape (even though this dissimilitude is small) induces some difference in the torques shapes.

The average torque is calculated. The average torque of the silicon steel motor is 49.47 Nm while the average torque of the amorphous alloy motor is 37.8 Nm. For a given supply voltage, the silicon steel motor develop a greater average torque than the amorphous alloy one.

4.5. Core Losses

A comparison of iron losses curves provided in Fig. 12. The iron loss of the amorphous alloy motor is much less than that of the silicon steel one.

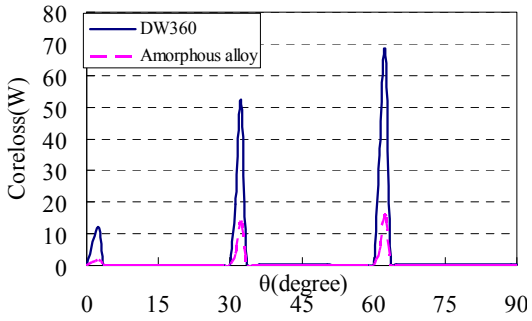

Fig. 12. Iron losses versus time at 50 Hz.

The rms core losses are calculated. The rms core loss of the silicon steel motor is about 18.76 W while the rms core loss of the amorphous alloy motor is about 197.44 μW. For a given supply voltage, the silicon steel motor develop a much smaller rms core losses than the amorphous alloy one.

5. Conclusions

This paper focuses on the performance analysis of a prototype amorphous alloys core SRM (100 W/100 rpm) for home appliance applications. With the help of response surface methodology (RSM) and the parameterized transient finite element analysis model of the sample SRM, the stator pole arc β_s, rotor pole arc β_r, the turn-on angle θ_{on} and turn-off angle θ_{off} of the sample SRM are optimized for reducing torque ripple. The magnetic fields distribution, the torque characteristics of the prototype machine are presented by using finite element analysis. The studies show that the amorphous alloys core SRM is potential to achieve high efficiency.

Acknowledgements

This work was supported in part by The National Natural Science Foundation of China (No. 51377008).

References

[1]. A. M. Omekanda, A new technique for multi-dimensional performance optimization of switched reluctance motors for vehicle propulsion, *IEEE Transactions on Industry Applications*, Vol. 39, No. 3, 2003, pp. 672-676.

[2]. K. Nakamura, T. Ono, H. Goto, T. Watanabe, O. Ichinokura, A novel switched reluctance motor with wound-cores put on stator and rotor poles, *IEEE Transactions on Magnetics*, Vol. 41, No. 10, 2005, pp. 3919-3921.

[3]. S. Inamura, T. Sakai, K. Sawa, A temperature rise analysis of switched reluctance motor due to the core and copper loss by FEM, *IEEE Transactions on Magnetics*, Vol. 39, No. 3, 2003, pp. 1554-1557.

[4]. H. Torkaman, and E. Afjei, FEM analysis of angular misalignment fault in SRM magnetostatic characteristics, *Progress in Electromagnetics Research*, Vol. 104, 2010, pp. 31-48.

[5]. H. Torkaman, and E. Afjei, Hybrid method of obtaining degrees of freedom for radial airgap length in SRM under normal and faulty conditions based on magnetostatic model, *Progress in Electromagnetics Research*, Vol. 100, 2010, pp. 37-54.

[6]. Huang Guozhi and Fu Fengli, Technical manual of Y2 series 3-phase induction motors, *China Machine Press*, Beijing, 2005, pp. 318-327.

[7]. K. Kariatsumari, The motor revolutions begins from home appliances: using washer/dryer technology in EVs, *Nikkei Electronics Asia*, May 2010.

[8]. Y. Guo, J. Zhu, D. G. Dorrell, Design and analysis of a claw pole permanent magnet motor with molded soft magnetic composite core, *IEEE Transactions on Magnetics*, Vol. 45, No. 10, October 2009, pp. 4582-4585.

[9]. Z. Wang, Y. Enomoto, M. Ito, R. Masaki, S. Morinaga, H. Itabashi, and S. Tanigawa, Development of a permanent magnet motor utilizing amorphous wound cores, *IEEE Transactions on Magnetics*, Vol. 46, Issue 2, February 2010, pp. 570-573.

[10]. Z. Wang, Y. Enomoto, M. Ito, R. Masaki, S. Morinaga, H. Itabashi, and S. Tanigawa, Development of an axial gap motor with amorphous metal cores, *IEEE Transactions on Industry Applications*, Vol. 47, No. 3, 2011, pp. 1293-1299.

[11]. M. Dems, K. Komeza, S. Wiak, T. Stec, The highly efficient three-phase small induction motors with stator cores made from amorphous iron, *The International Journal for Computation and Mathematics in Electrical and Electronic Engineering*, Vol. 23, No. 3, 2004, pp. 625-632.

[12]. Yuan Liqing, Zhong Degang, Chen Yongxiao, Amorphous metal motor and its prospects, *Small & Special Electrical Machines*, No. 4, 2004, pp. 34-36. (in Chinese).

[13]. E. Afjei, and H. Torkaman, Comparison of two types of dual layer generator in field assisted mode utilizing 3D-FEM and experimental verification, *Progress in Electromagnetics Research B*, Vol. 23, 2010, pp. 293-309.

[14]. H. Torkaman, and E. Afjei, Magnetostatic field analysis regarding the effects of dynamic eccentricity in switched reluctance motor, *Progress in Electromagnetics Research M*, Vol. 8, 2009, pp. 163-180.

[15]. Zhan Qionghua, Switched reluctance motor, *Huazhong University of Science Press*, Hubei, 1992.

2014 Copyright ©, International Frequency Sensor Association (IFSA) Publishing, S. L. All rights reserved. (http://www.sensorsportal.com)